Design of a Broadband Erbium-Doped Fluoroindate Fiber Laser Emitting Up to 3.91 μm

Mario Christian Falconi, Antonella Maria Loconsole, Andrea Annunziato, Solenn Cozic, Samuel Poulain, and Francesco Prudenzano, *Member, IEEE*

***Abstract*—In this paper, for the first time, an erbium-doped fluoroindate fiber laser emitting up to 3.91 μm is designed and optimized by means of a numerical investigation performed via a home-made computer code. It is cladding pumped with red light at 635 nm. The employed fiber is commercially available from Le Verre Fluoré and exhibits a double D-shaped geometry. Continuous-wave laser emission is obtained thanks to the population inversion between the $^4F_{9/2}$ and $^4I_{9/2}$ energy levels. The model takes into account measured spectroscopic parameters for the absorption, stimulated emission and spontaneous decay processes. The device performance is investigated by varying several parameters, such as the input pump power, the fiber length, the dopant concentration, the output mirror reflectivity and the signal wavelength. The proposed device is very versatile and is optimized for different scenarios, including: the shortest fiber, the highest output power and the lowest threshold. Simulation results show that the best performance in terms of emission bandwidth is obtained for the laser with the lowest threshold, i.e., only 25 mW, predicting a broadband coherent emission in the 3.25–3.91 μm wavelength range and paving the way to the fabrication of a low-cost and easy-to-pump middle infrared fiber laser.**

***Index Terms*—Double D-shaped fiber, erbium, fiber laser, fluoroindate glass, middle infrared.**

I. Introduction

In recent years, rare-earth-doped fluoroindate glass (IFG) has been the subject of numerous spectroscopic studies,

Manuscript received 8 February 2023; revised 27 March 2023 and 29 April 2023; accepted 8 May 2023. Date of publication 11 May 2023; date of current version 19 September 2023. This work was supported in part by the European Union through the Italian National Recovery and Resilience Plan of NextGenerationEU, with particular reference to the partnership on Telecommunications of the Future PE00000001 - program "RESTART", CUP: D93C22000910001 - DREAMS - Antennas and Devices foR mixing, dEtection And Manipulation of mmWaves, in part by PON R&I 2014-2020 AIM: Attraction and International Mobility Line 1 under Grant AIM1895471-3, in part by MIUR Agriculture Green and Digital – AGREED, under Grants PNR 2015/20 and ARS01_00254, and in part by H2020-ICT-37-2020 Photonic Accurate and Portable Sensor Systems Exploiting Photo-Acoustic and Photo-Thermal Based Spectroscopy for Real-Time Outdoor Air Pollution Monitoring – PASSEPARTOUT, under Grant 101016956. *(Corresponding author: Francesco Prudenzano.)*

This work did not involve human subjects or animals in its research.

Mario Christian Falconi, Antonella Maria Loconsole, Andrea Annunziato, and Francesco Prudenzano are with the Department of Electrical and Information Engineering, Politecnico di Bari, 70125 Bari, Italy (e-mail: mariochristian.falconi@poliba.it; antonellamaria.loconsole@poliba.it; andrea.annunziato@poliba.it; francesco.prudenzano@poliba.it).

Solenn Cozic and Samuel Poulain are with the Le Verre Fluoré, 35170 Bruz, France (e-mail: solenn.cozic@leverrefluore.eu; samuel.poulain@leverrefluore.eu).

Color versions of one or more figures in this article are available at https://doi.org/10.1109/JLT.2023.3275168.

Digital Object Identifier 10.1109/JLT.2023.3275168

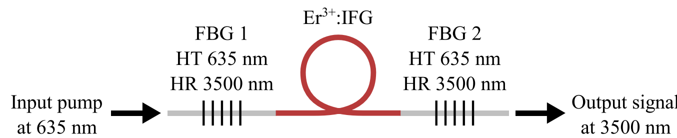

Fig. 1. Schematic of the device.

aimed to explore middle infrared (Mid-IR) emission at wavelengths as high as $\lambda = 5.5$ μm [1], [2], [3], [4], [5], [6], [7], [8], [9], [10], [11], [12], [13], [14], [15], [16], [17], [18], [19]. Its typical chemical composition is InF_3-ZnF_2-SrF_2-BaF_2 and it offers better thermal stability with respect to fluorozirconate glass and a broad optical transmission window going from the ultraviolet to the middle infrared. The main advantages which make its employment as active medium feasible are the low phonon energy ($\approx$510 cm^{-1}) and the ability to accommodate high dopant concentrations (up to 10 mol%).

In the literature, both continuous-wave (CW) and pulsed fluoroindate fiber lasers were proposed. In [4], a CW holmium-doped fluoroindate fiber laser was successfully demonstrated. It was cladding pumped at $\lambda_p = 888$ nm and emitted almost 200 mW of optical power at $\lambda_s = 3.92$ μm. The related slope efficiency was close to 10%. In [6], a gain-switched heavily-holmium-doped fluoroindate fiber laser emitting at the same wavelength was proposed and optimized. Pulses with a duration $\tau_{FWHM} = 72.55$ ns and an energy E = 1.21 μJ were predicted. The related optical-to-optical conversion efficiency was about $\eta_c = 4\%$. Stable single pulse operation up to a repetition rate $f_R = 200$ kHz was simulated. In [12], a CW fiber laser exploiting a fluoroindate glass co-doped with holmium and neodymium was investigated. It was pumped at $\lambda_p = 808$ nm and emitted at $\lambda_s = 3.92$ μm. By tailoring the length of the fiber and the concentrations of both dopants, a threshold power as low as $P_{th} = 200$ mW and a slope efficiency close to $\eta_s = 16.67\%$ were predicted.

In this paper, for the first time to the best of our knowledge, a widely tunable erbium-doped fluoroindate CW fiber laser providing a bandwidth of almost BW = 659 nm, from λ_s = 3.25 μm up to λ_s = 3.91 μm, is proposed and optimized. The geometry of the fiber laser section corresponds, with the exception of the employed rare earth, to that of a commercially available fluoroindate fiber produced by Le Verre Fluoré, having a double D-shaped geometry. The laser is cladding pumped with red light at $\lambda_p = 635$ nm (see Fig. 1), which makes it very attractive since low-cost red laser diodes (e.g., Thorlabs L637G1) can be employed. Moreover, a fluoroindate fiber combiner [20]

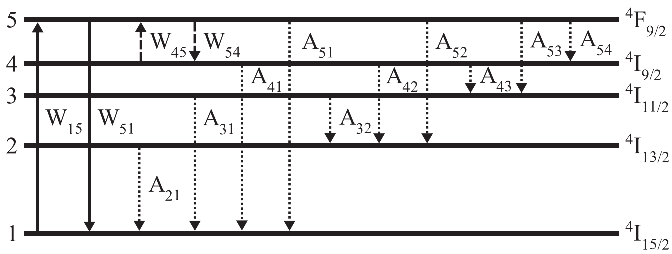

Fig. 2. Energy levels scheme for the Er^{3+}: IFG system.

could be used if a higher pump power is desired, maintaining a low cost. Potential applications include, but are not limited to, environmental monitoring (e.g., by exploiting the absorption peaks of air pollutants in the middle infrared), remote sensing, biomedicine, optical communications and polymer processing [21], [22], [23].

II. Theory

The pumping scheme for the Er^{3+}:IFG system exploits an optical beam at $\lambda_p = 635$ nm to promote electrons from the ground state $^4I_{15/2}$ to the upper laser level $^4F_{9/2}$, as shown in Fig. 2. The complete model consists of 5 energy levels [16], including the lower laser level $^4I_{9/2}$ and two intermediate levels ($^4I_{13/2}$ and $^4I_{11/2}$). The considered optical transitions are the following: pump absorption (upward solid arrow), pump stimulated emission (downward solid arrow), signal absorption (upward dashed arrow), signal stimulated emission (downward dashed arrow), radiative decays (downward dotted arrows). The employment of a laser transition that does not involve the ground state helps to avoid the phenomenon of signal reabsorption, once the pump is exhausted. Pump excited state absorption (ESA) occurring between the $^4I_{13/2}$ and the ($^4F_{3/2}$, $^4F_{5/2}$) energy levels is neglected since, according to spectroscopic studies [24], the lifetime of the ($^4F_{3/2}$, $^4F_{5/2}$) level is rather short and the branching ratio between it and the ground state is over 61%. This implies that the majority of electrons promoted by pump ESA decay to the ground state and are available again for exciting the upper laser level. Furthermore, potential non-radiative decay from the ($^4F_{3/2}$, $^4F_{5/2}$) energy level might have a positive effect on the population of the $^4F_{9/2}$ level, leading to an improvement in the laser efficiency.

In order to study the population inversion with the aim of obtaining laser emission around $\lambda_s = 3.5$ μm, the following rate equations for the energy levels populations N_1, …, N_5 are written:

$$\frac{\partial N_5}{\partial t} = W_{15}N_1 - W_{51}N_5 + W_{45}N_4 - W_{54}N_5 - (A_{51} + A_{52} + A_{53} + A_{54})\, N_5 \tag{1a}$$

$$\frac{\partial N_4}{\partial t} = -W_{45}N_4 + W_{54}N_5 + A_{54}N_5 - (A_{43} + A_{42} + A_{41})\, N_4 \tag{1b}$$

$$\frac{\partial N_3}{\partial t} = -(A_{32} + A_{31})\, N_3 + A_{43}N_4 + A_{53}N_5 \tag{1c}$$

$$\frac{\partial N_2}{\partial t} = -A_{21}N_2 + A_{32}N_3 + A_{42}N_4 + A_{52}N_5 \tag{1d}$$

$$\frac{\partial N_1}{\partial t} = -W_{15}N_1 + W_{51}N_5 + A_{21}N_2 + A_{31}N_3 + A_{41}N_4 + A_{51}N_5 \tag{1e}$$

The system (1a)–(1e) is solved under stationary conditions, i.e., all time derivatives vanish, and by imposing that the sum of the populations is equal to the erbium concentration N_{Er}:

$$N_1 + N_2 + N_3 + N_4 + N_5 = N_{Er} \tag{2}$$

The pump and signal transition rates are calculated as follows:

$$W_{15} = \frac{\sigma_{15}(\lambda_p)}{\frac{hc_0}{\lambda_p}} \left[P_p^+(z) + P_p^-(z)\right] i_p \tag{3}$$

$$W_{51} = \frac{\sigma_{51}(\lambda_p)}{\frac{hc_0}{\lambda_p}} \left[P_p^+(z) + P_p^-(z)\right] i_p \tag{4}$$

$$W_{45} = \frac{\sigma_{45}(\lambda_s)}{\frac{hc_0}{\lambda_s}} \sum_{k=1}^{6} \left[P_{s,k}^+(z) + P_{s,k}^-(z)\right] i_{s,k}(x,y) \tag{5}$$

$$W_{54} = \frac{\sigma_{54}(\lambda_s)}{\frac{hc_0}{\lambda_s}} \sum_{k=1}^{6} \left[P_{s,k}^+(z) + P_{s,k}^-(z)\right] i_{s,k}(x,y) \tag{6}$$

where c_0 is the speed of light in vacuum, h the is Planck constant, λ_p is the pump wavelength, λ_s is the signal wavelength, the cross section at the wavelength λ for the i $\rightarrow$ j transition is denoted by $\sigma_{ij}(\lambda)$, $P_p^{\pm}$ is the forward (plus sign) and backward (minus sign) pump power, $P_{s,k}^{\pm}$ is the forward (plus sign) and backward (minus sign) signal power of the k-th guided mode, $i_{s,k}$ is the normalized intensity distribution of the signal for the k-th guided mode. The normalized intensity distribution i_p of the pump is calculated by considering the inner cladding shape of the double D-shaped fiber and assuming that the pump power is uniformly distributed in both the core and the inner cladding:

$$i_p = \frac{1}{A_p} = \left[\frac{d_{cut}}{2}\sqrt{d_{icl}^2 - d_{cut}^2} + \frac{d_{icl}^2}{2}\sin^{-1}\left(\frac{d_{cut}}{d_{icl}}\right)\right]^{-1} \tag{7}$$

where d_{icl} is the diameter of the inner cladding, which is cut by two parallel lines at a distance d_{cut}, and A_p is the sum of the core and the inner cladding areas. The radiative decay rate A_{ij} for the i $\rightarrow$ j transition is given by the ratio between the branching ratio β_{ij} of the transition and the lifetime τ_i of the starting energy level:

$$A_{ij} = \frac{\beta_{ij}}{\tau_i} \tag{8}$$

The dependence of the pump and signals powers on the longitudinal position along the fiber is given by the power propagation equations [25], [26]. For k guided modes propagating at the signal wavelength, 2 × k equations are needed, taking into account both propagation directions:

$$\frac{dP_p^+}{dz} = \left[g_p(z) - \alpha(\lambda_p)\right] P_p^+(z) \tag{9a}$$

$$\frac{dP_p^-}{dz} = -\left[g_p(z) - \alpha(\lambda_p)\right] P_p^-(z) \quad (9b)$$

$$\frac{dP_{s,k}^+}{dz} = \left[g_{s,k}(z) - \alpha(\lambda_s)\right] P_{s,k}^+(z) \quad (9c)$$

$$\frac{dP_{s,k}^-}{dz} = -\left[g_{s,k}(z) - \alpha(\lambda_s)\right] P_{s,k}^-(z) \quad (9d)$$

where $\alpha(\lambda)$ is the wavelength-dependent background loss and the gain coefficients are given by the overlap integrals, over the doped core region Ω_d, between the populations and the normalized intensity distributions:

$$g_p(z) = -\sigma_{15}(\lambda_p)\int_{\Omega_d} N_1 i_p dxdy + \sigma_{51}(\lambda_p)\int_{\Omega_d} N_5 i_p dxdy \quad (10)$$

$$g_{s,k}(z) = -\sigma_{45}(\lambda_s)\int_{\Omega_d} N_4 i_{s,k}(x,y)\,dxdy + \sigma_{54}(\lambda_s)\int_{\Omega_d} N_5 i_{s,k}(x,y)\,dxdy \quad (11)$$

The boundary conditions for the differential equations system (9a)–(9d) are related to the forward/backward input pump power injected into the fiber and the two fiber Bragg gratings (FBGs) employed as mirrors:

$$P_p^+(0) = P_{p0}^+ \quad (12a)$$

$$P_p^-(L) = P_{p0}^- \quad (12b)$$

$$P_{s,k}^+(0) = R_1\, P_{s,k}^-(0) \quad (12c)$$

$$P_{s,k}^-(L) = R_2\, P_{s,k}^+(L) \quad (12d)$$

where L is the fiber length, $P_{p0}\pm$ is the forward (plus sign) and backward (minus sign) input pump power, R_1 is input FBG reflectivity and R_2 is the output FBG reflectivity. The output signal power P_{out} of the laser is given by sum of the transmitted powers of each forward signal mode:

$$P_{out} = (1 - R_2)\sum_k P_{s,k}^+(L) \quad (13)$$

By exploiting (13), it is also possible to evaluate the slope efficiency η_s and the threshold power P_{th}. The developed model is very versatile and can be potentially adapted to simulate amplifiers [27] and pulsed lasers [28], [29], [30], [31] or to be employed in machine learning systems [32] by appropriately modifying the equations and the boundary conditions.

III. Laser Design

The employed active fluoroindate fiber is commercially available from Le Verre Fluoré. Its section has a double D-shaped geometry. In particular, the core diameter is $d_{co} = 16$ μm and the inner cladding diameter is $d_{icl} = 100$ μm. The distance at which the inner cladding is cut is $d_{cut} = 90$ μm. The total area calculated via (7) is $A_p = 7560$ μm^2, leading to a normalized pump intensity distribution $i_p = 132.3$ $\mu W/\mu m^2$. The glass refractive index is close to $n_{IFG}(\lambda_s) = 1.5$ at the signal wavelength $\lambda_s = 3.5$ μm and $n_{IFG}(\lambda_p) = 1.51$ at the pump wavelength $\lambda_p = 635$ nm [20]. The core/inner cladding and the inner/outer claddings numerical apertures are $NA_1 = 0.2$ and $NA_2 = 0.5$, respectively. The background losses at the pump and signal wavelengths are $\alpha(\lambda_p) = 0.25$ dB/m and $\alpha(\lambda_s) = 0.0045$ dB/m, respectively. Fig. 3 shows the longitudinal field components and the effective mode indices for the guided modes inside the core of the fluoroindate fiber at the signal wavelength $\lambda_s = 3.5$ μm, obtained through a finite element method (FEM) analysis. Table I reports the spectroscopic parameters for the erbium ions in the fluoroindate glass, extracted from the literature [16], [24], [33]. The pump absorption cross section is assumed equal to the emission cross section. The design of the laser is performed by studying the output signal power, when the dopant concentration increases from a low to a high value in the range $N_{Er} = 2 \times 10^{25}$-$8 \times 10^{25}$ ions/m^3 (see Figs. 4–6). The input mirror reflectivity is kept fixed to $R_1 = 99\%$, in agreement with the recent advances on inscription of FBGs in fluoroindate fibers [34]. Co-directional pumping is considered with an input pump power equal to $P_{p0}^+ = P_{p0} = 1$ W. It is worth noting that a positive optical gain was achieved only for the fundamental mode HE_{11}, even with input pump powers up to $P_{p0} = 10$ W, thanks to its higher overlap coefficient compared with those of the higher order modes. In the following, step sizes equal to $\Delta L = 10$ cm and $\Delta R_2 = 2\%$ are assumed for discretizing the fiber length L and the output mirror reflectivity R_2, respectively.

TABLE I
Spectroscopic Parameters for the Erbium-Doped Fluoroindate Glass

Parameter	Value	Description
λ_p	635 nm	Pump wavelength
λ_s	3.5 µm	Signal wavelength
λ_c	4.2 µm	Fiber cut-off wavelength
$\sigma_{15}(\lambda_p)$	1.1547×10^{-24} m^2	Pump absorption cross section
$\sigma_{51}(\lambda_p)$	1.1547×10^{-24} m^2 [24,33]	Pump emission cross section
$\sigma_{45}(\lambda_s)$	4.6058×10^{-26} m^2 [16]	Signal absorption cross section
$\sigma_{54}(\lambda_s)$	4.8468×10^{-26} m^2 [16]	Signal emission cross section
τ_2	12.57 ms [16]	$^4I_{13/2}$ energy level lifetime
τ_3	10.49 ms [16]	$^4I_{11/2}$ energy level lifetime
τ_4	8.33 ms [16]	$^4I_{9/2}$ energy level lifetime
τ_5	1.04 ms [16]	$^4F_{9/2}$ energy level lifetime
β_{21}	100% [16]	$^4I_{13/2} \rightarrow {}^4I_{15/2}$ branching ratio
β_{32}	14.23% [16]	$^4I_{11/2} \rightarrow {}^4I_{13/2}$ branching ratio
β_{31}	85.77% [16]	$^4I_{11/2} \rightarrow {}^4I_{15/2}$ branching ratio
β_{43}	0.53% [16]	$^4I_{9/2} \rightarrow {}^4I_{11/2}$ branching ratio
β_{42}	22.80% [16]	$^4I_{9/2} \rightarrow {}^4I_{13/2}$ branching ratio
β_{41}	76.67% [16]	$^4I_{9/2} \rightarrow {}^4I_{15/2}$ branching ratio
β_{54}	0.21% [16]	$^4F_{9/2} \rightarrow {}^4I_{9/2}$ branching ratio
β_{53}	4.38% [16]	$^4F_{9/2} \rightarrow {}^4I_{11/2}$ branching ratio
β_{52}	4.99% [16]	$^4F_{9/2} \rightarrow {}^4I_{13/2}$ branching ratio
β_{51}	90.43% [16]	$^4F_{9/2} \rightarrow {}^4I_{15/2}$ branching ratio

Fig. 4 shows the output signal power P_{out} as a function of the fiber length L and the output mirror reflectivity R_2, for a low dopant concentration $N_{Er} = 2 \times 10^{25}$ ions/m^3. Output powers of at least $P_{out} = 1$ mW are obtained for $L = 0.5$ m and $R_2 = 97\%$. Increasing the fiber length and reducing the reflectivity yields similar output powers. Better results are obtained by increasing both L and R_2. The maximum output power $P_{out} = 10$ mW is achieved only for very long fibers, i.e., $L > 4.6$ m, requiring an output mirror reflectivity around $R_2 \approx 90\%$.

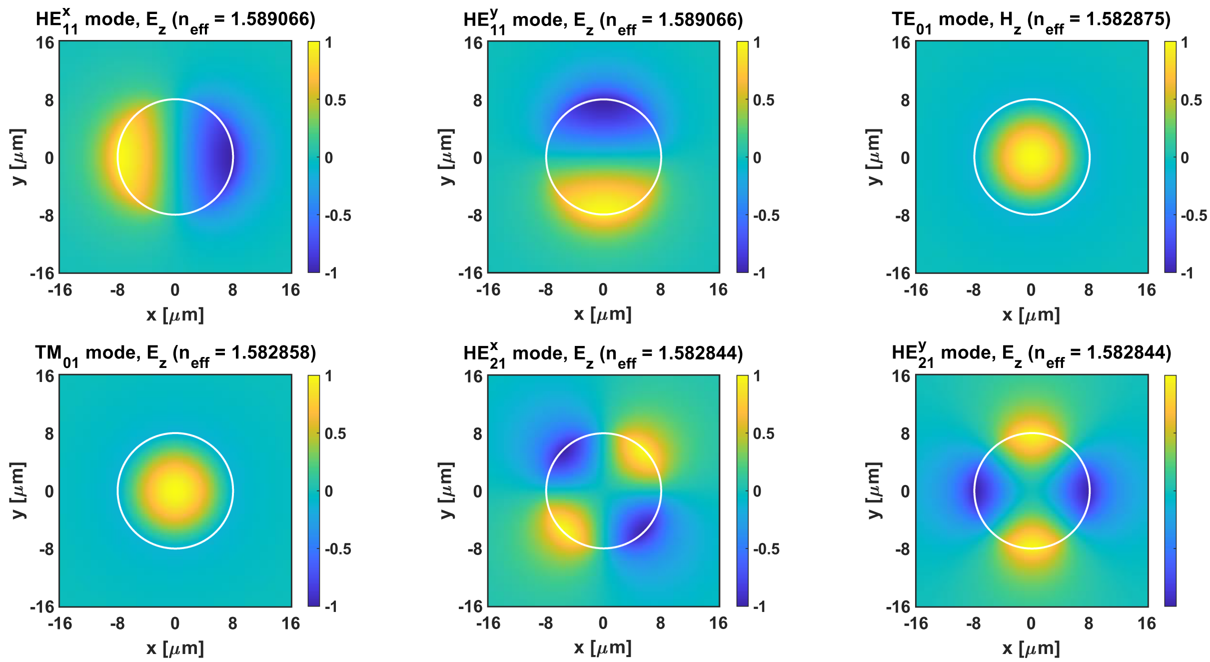

Fig. 3. Longitudinal components E_z/H_z and effective mode indices for the six guided optical modes of the double D-shaped fluoroindate fiber at the signal wavelength $\lambda_s = 3500$ nm. The fiber core is represented by the white circle.

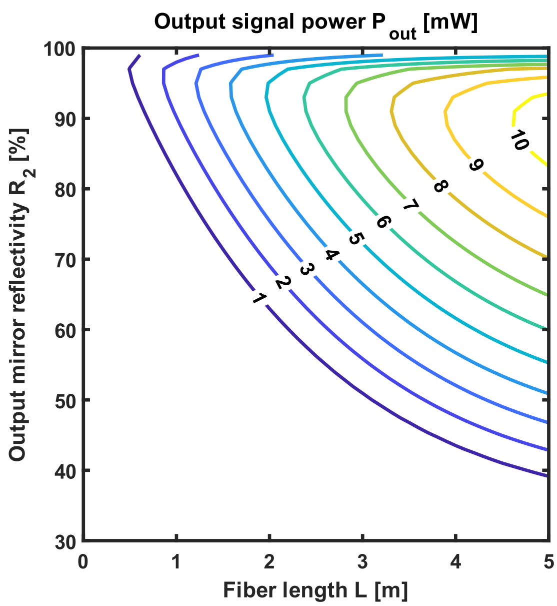

Fig. 4. Output signal power P_{out} as a function of the fiber length L and the output mirror reflectivity R_2. Input pump power $P_{p0} = 1$ W, dopant concentration $N_{Er} = 2 \times 10^{25}$ ions/m^3, input mirror reflectivity $R_1 = 99\%$.

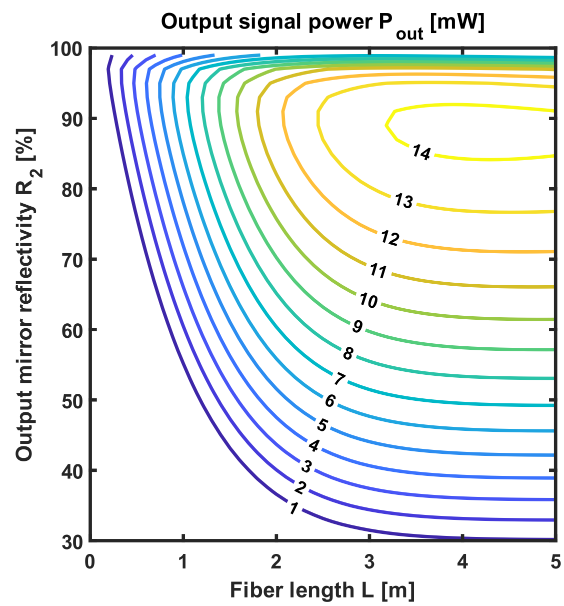

Fig. 5. Output signal power P_{out} as a function of the fiber length L and the output mirror reflectivity R_2. Input pump power $P_{p0} = 1$ W, dopant concentration $N_{Er} = 5 \times 10^{25}$ ions/m^3, input mirror reflectivity $R_1 = 99\%$.

Fig. 5 shows the output signal power P_{out} as a function of the fiber length L and the output mirror reflectivity R_2, for an intermediate dopant concentration $N_{Er} = 5 \times 10^{25}$ ions/m^3. In this case, thanks to the higher optical gain, similar output powers are obtained with shorter fibers and smaller reflectivities. It is also apparent that, for lengths greater than L = 4 m, the signal power is almost independent of the fiber length value. The shortest fiber length providing at least $P_{out} = 1$ mW is close to L = 0.2 m, again with $R_2 = 97\%$. The maximum output power $P_{out} = 14$ mW is achieved for the fiber length L = 3.2 m, with an output mirror reflectivity around $R_2 \approx 88\%$.

Fig. 6 shows the output signal power P_{out} as a function of the fiber length L and the output mirror reflectivity R_2, for a high dopant concentration $N_{Er} = 8 \times 10^{25}$ ions/m^3. Although an even higher concentration improves the overall efficiency, the benefit is marginal. In fact, the achievable power levels are very close to the previous case and saturation already occurs for lengths greater than L = 2.5 m. The maximum output power increases

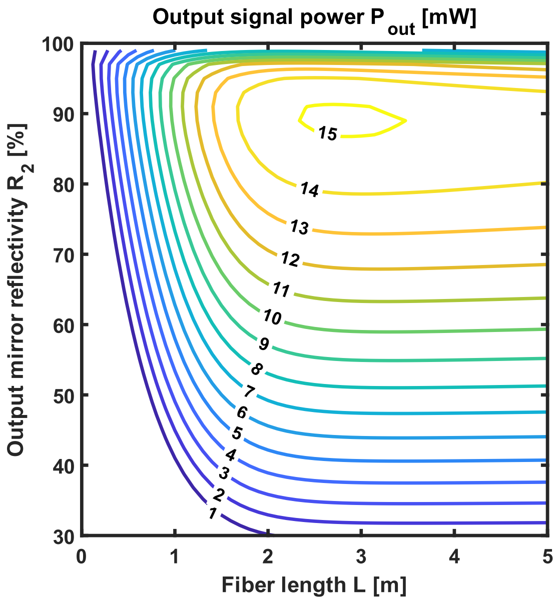

Fig. 6. Output signal power P_{out} as a function of the fiber length L and the output mirror reflectivity R_2. Input pump power $P_{p0} = 1$ W, dopant concentration $N_{Er} = 8 \times 10^{25}$ ions/m^3, input mirror reflectivity $R_1 = 99\%$.

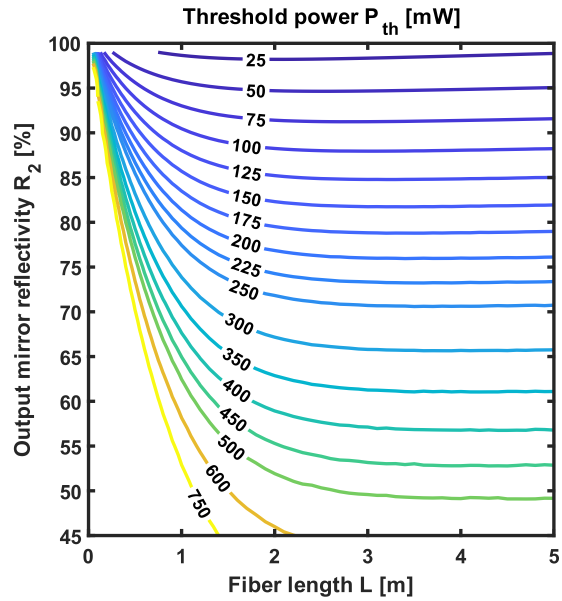

Fig. 7. Threshold power P_{th} as a function of the fiber length L and the output mirror reflectivity R_2. Dopant concentration $N_{Er} = 5 \times 10^{25}$ ions/m^3, input mirror reflectivity $R_1 = 99\%$.

by only one mW, reaching $P_{out} = 15$ mW when the fiber length is $L = 2.4$ m and the output reflectivity is $R_2 = 89\%$. In view of this, it was decided to keep the dopant concentration from now on at the intermediate value of $N_{Er} = 5 \times 10^{25}$ ions/m^3 ≈ 0.26 mol%, also to avoid the occurrence of concentration quenching phenomena and detrimental nonlinear effects. It is worth noting that in [16] no quenching in the $\lambda = 3.5$ μm emission spectrum was observed for Er^{3+} concentrations up to 9 mol%.

Another important feature for a laser is the threshold power P_{th}, here defined as the input pump power value required to obtain a signal power of at least $P_{out} = 10$ μW. Fig. 7 shows the threshold power P_{th} as a function of the fiber length L and the output mirror reflectivity R_2. The threshold power strongly depends on the output reflectivity, but becomes almost insensitive to the length for fibers longer than $L = 2.5$ m. Similar thresholds are obtained by simultaneously increasing the fiber length and reducing the output reflectivity. The mirror reflectivity must be kept higher than $R_2 = 86\%$ if threshold powers less than $P_{th} =$ 100 mW are desired. On the other hand, if the mirror reflectivity is less than $R_2 = 49\%$, at least half a watt of pump is needed to achieve lasing.

IV. Refinement

According to the results reported in Section III, it is apparent that identifying a unique configuration that simultaneously provides the highest output power and the lowest threshold power is not possible. Moreover, no information regarding the laser bandwidth can be inferred. To overcome these issues, three different scenarios are considered for optimizing the device: (I) shortest fiber, (II) highest output power and (III) lowest threshold. In the first scenario, the goal is to shorten the fiber as much as possible in order to obtain a coherent light source in the middle infrared which is very compact and, hence, affordable. It was accomplished by selecting, in Fig. 5, the curve corresponding to the shortest fiber, i.e., $L = 19.3$ cm, still proving an output power of $P_{out} = 1$ mW. The required mirror reflectivity is $R_2 =$ 97%. In the second scenario, the goal is to increase the signal power, for the same input pump power, as much as possible in order to obtain the laser with the highest output power, exploiting most of the pump power. It was accomplished by selecting, in Fig. 5, the point at the center of the region bounded by the yellow contour line, having coordinates $L = 4.3$ m and $R_2 = 88.5\%$ and yielding the maximum signal power $P_{out} = 14.25$ mW. In the last scenario, the goal is to decrease the threshold power as much as possible in order to obtain a device which is easy to pump with low-cost red laser diodes. It was accomplished by selecting, in Fig. 7, the curve corresponding to the lowest threshold power, i.e., $P_{th} = 25$ mW, with a decent trade-off between the fiber length, equal to $L = 2.1$ m, and the mirror reflectivity, equal to $R_2 = 98.2\%$.

Fig. 8 shows the output signal power P_{out} as a function of the input pump power P_{p0} for the three aforementioned optimization scenarios. It allows for evaluating the slope efficiency η_s and the threshold power P_{th} for each configuration. In particular, the slope efficiencies for the optimization scenarios (I), (II) and (III) are rather low, respectively $\eta_s = 0.2\%$, $\eta_s = 1.6\%$ and $\eta_s = 1\%$. On the other hand, the threshold powers are $P_{th} = 127$ mW, P_{th} $= 97$ mW and $P_{th} = 25$ mW, respectively.

The carried out final investigation concerns the laser bandwidth, which was studied by varying the signal wavelength. The dependence of the background loss on the wavelength is taken into account even if it is typically lower than $\alpha(\lambda_s) = 0.009$ dB/m and could be neglected. Fig. 9 shows the output signal power P_{out} as a function of the signal wavelength λ_s, again for the three optimization scenarios. The device optimized for

TABLE II
PARAMETERS OF THE FIBER LASER OPTIMIZED FOR DIFFERENT SCENARIOS

Parameter	Optimization Scenario I	Optimization Scenario II	Optimization Scenario III	Description
L	19.3 cm	4.3 m	2.1 m	Fiber length
N_{Er}	5×10^{25} ions/m^3	5×10^{25} ions/m^3	5×10^{25} ions/m^3	Dopant concentration
R_1	99%	99%	99%	Input mirror reflectivity
R_2	97%	88.5%	98.2%	Output mirror reflectivity
λ_s	3.62 µm	3.73 µm	3.8 µm	Central wavelength
P_{out}	1.1 mW	22.5 mW	15.5 mW	Output power (at central wavelength)
BW	440 nm	545 nm	659 nm	10-dB bandwidth
η_s	0.2%	1.6%	1%	Slope efficiency (at λ_s = 3.5 µm)
P_{th}	127 mW	97 mW	25 mW	Threshold power (at λ_s = 3.5 µm)

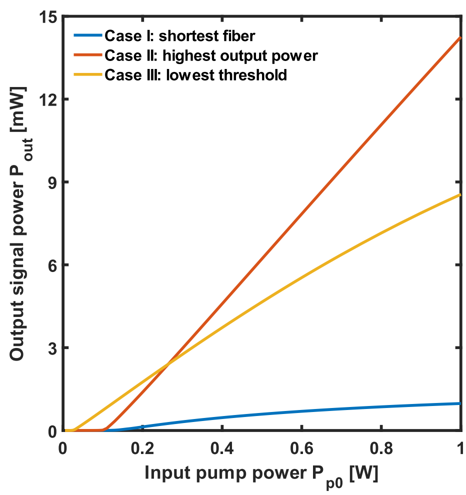

Fig. 8. Output signal power P_{out} as a function of the input pump power P_{p0} for three optimization scenarios: (I) shortest fiber, (II) highest output power and (III) lowest threshold. Dopant concentration $N_{Er} = 5 \times 10^{25}$ ions/m^3, input mirror reflectivity $R_1 = 99\%$.

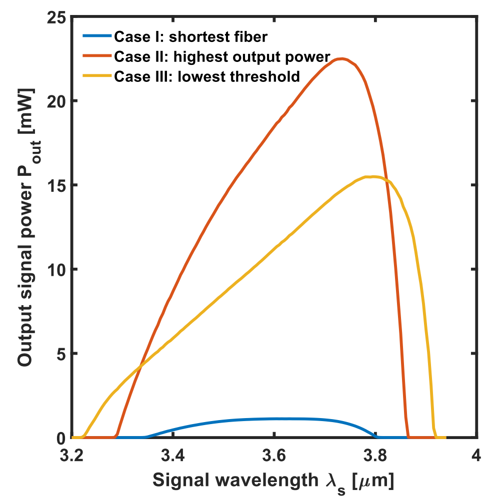

Fig. 9. Output signal power P_{out} as a function of the signal wavelength λ_s for three optimization scenarios: (I) shortest fiber, (II) highest output power and (III) lowest threshold. Input pump power $P_{p0} = 1$ W, dopant concentration $N_{Er} = 5 \times 10^{25}$ ions/m^3, input mirror reflectivity $R_1 = 99\%$.

the scenario (I) exhibits the lowest output power $P_{out} = 1.1$ mW at the wavelength $\lambda_s = 3.62$ µm. This was to be expected, since a short fiber limits the overall optical gain. However, this configuration provides the flattest spectral response, with a 10-dB bandwidth of BW = 440 nm. The device optimized for the scenario (II) exhibits the highest output power $P_{out} = 22.5$ mW at the wavelength $\lambda_s = 3.73$ µm, with an apparent benefit. The 10-dB bandwidth increases to BW = 545 nm. Lastly, the device optimized for the scenario (III) exhibits an intermediate output power $P_{out} = 15.5$ mW at the wavelength $\lambda_s = 3.8$ µm. This is the configuration which provides the widest 10-dB bandwidth BW = 659 nm, covering the spectral range $\lambda =$ 3255-3913 nm. This is because a lower threshold power makes it easier to obtain a positive net gain at wavelengths far from the central wavelength. It is also worth noting that single-mode operation still occurred for all three optimization scenarios in the entire wavelength range. Table II summarizes in a compact form the results exposed in this Section. For a comparison, in [35] a CW erbium-doped ZBLAN fiber laser pumped at $\lambda_p = 658$ nm emitted up to $P_{out} = 203$ mW at $\lambda_s = 3462$ nm by employing a much higher input pump power $P_{p0} = 8.6$ W. The fiber was L = 2.15 m long, with a pretty high erbium concentration $N_{Er} = 7$ mol%. The measured slope efficiency was about $\eta_s = 3.8\%$, with a threshold power of about $P_{th} = 3.4$ W. Even though the device here proposed exhibits a slightly worse slope efficiency ($\eta_s =$ 1.6% for the Optimization Scenario II), numerical simulations predict much better threshold powers (only $P_{th} = 25$ mW for the Optimization Scenario III) with very low doping levels ($N_{Er} = 5 \times 10^{25}$ ions/m$^3 \approx 0.26$ mol%).

V. CONCLUSION

For the first time, a CW erbium-doped fluoroindate fiber laser emitting in the middle infrared is accurately designed and optimized for different scenarios. Its performance was deeply investigated by studying the output signal power, the threshold power, the slope efficiency and the emission bandwidth. Among the three optimized configurations, the one with the lowest threshold power offers the widest 10-dB bandwidth of 659 nm, emitting 15.5 mW of optical power at 3800 nm and covering the spectral range from 3255 nm to 3913 nm. Despite the low slope efficiency, the obtained results are promising and encourage the fabrication of the proposed fiber laser, which could find applications in environmental monitoring, remote sensing, biomedicine and optical communications. The designed laser is attractive since it exploits an optical fiber available on the market from Le

Verre Fluoré and can be easily pumped at 635 nm with low-cost red laser diodes.

REFERENCES

[1] L. Gomes et al., "The basic spectroscopic parameters of Ho^{3+}-doped fluoroindate glass for emission at 3.9 μm," *Opt. Mater.*, vol. 60, pp. 618–626, Oct. 2016, doi: 10.1016/j.optmat.2016.08.019.

[2] M. R. Majewski, R. I. Woodward, J.-Y. Carree, S. Poulain, M. Poulain, and S. D. Jackson, "Emission beyond 4 μm and mid-infrared lasing in a dysprosium-doped indium fluoride (InF_3) fiber," *Opt. Lett.*, vol. 43, no. 8, pp. 1926–1929, Apr. 2018, doi: 10.1364/OL.43.001926.

[3] T. Castro, D. Manzani, and S. J. L. Ribeiro, "Up-conversion mechanisms in Er^{3+}-doped fluoroindate glasses under 1550 nm excitation for enhancing photocurrent of crystalline silicon solar cell," *J. Lumin.*, vol. 200, pp. 260–264, Aug. 2018, doi: 10.1016/j.jlumin.2018.04.028.

[4] F. Maes et al., "Room-temperature fiber laser at 3.92 μm," *Optica*, vol. 5, no. 7, pp. 761–764, Jul. 2018, doi: 10.1364/OPTICA.5.000761.

[5] R. Wang et al., "Enhancement mechanisms of Tm^{3+}-codoping on 2 μm emission in Ho^{3+} doped fluoroindate glasses under 888 nm laser excitation," *Ceram. Int.*, vol. 46, no. 5, pp. 6973–6977, Apr. 2020, doi: 10.1016/j.ceramint.2019.11.108.

[6] A. M. Loconsole, M. C. Falconi, V. Portosi, and F. Prudenzano, "Numerical design of a gain-switched pulsed laser at 3.92 μm wavelength based on a Ho^{3+}-doped fluoroindate fiber," *J. Light. Technol.*, vol. 39, no. 10, pp. 3276–3283, May 2021, doi: 10.1109/JLT.2021.3064764.

[7] M. Kochanowicz et al., "Near-IR and mid-IR luminescence and energy transfer in fuoroindate glasses co-doped with Er^{3+}/Tm^{3+}," *Opt. Mater. Exp.*, vol. 9, no. 12, pp. 4772–4781, Dec. 2019, doi: 10.1364/OME.9.004772.

[8] R. Wang et al., "3.9 μm emission and energy transfer in ultra-low OH^-, Ho^{3+}/Nd^{3+} co-doped fluoroindate glasses," *J. Lumin.*, vol. 225, Sep. 2020, Art. no. 117363, doi: 10.1016/j.jlumin.2020.117363.

[9] M. Kochanowicz et al., "Sensitization of Ho^{3+} - doped fluoroindate glasses for near and mid-infrared emission," *Opt. Mater.*, vol. 101, Mar. 2020, Art. no. 109707, doi: 10.1016/j.optmat.2020.109707.

[10] M. Kochanowicz et al., "Structure, luminescence and energy transfer of fuoroindate glasses codoped with Er^{3+}/Ho^{3+}," *Ceram. Int.*, vol. 46, no. 16, pp. 26403–26409, Feb. 2020, doi: 10.1016/j.ceramint.2020.02.210.

[11] W. A. Pisarski et al., "Fluoroindate glasses co–doped with Pr^{3+}/Er^{3+} for near–infrared luminescence applications," *Sci. Rep.*, vol. 10, Dec. 2020, Art. no. 21105, doi: 10.1038/s41598-020-77943-w.

[12] A. M. Loconsole, M. C. Falconi, A. Annunziato, S. Cozic, S. Poulain, and F. Prudenzano, "Design of a mid-IR laser based on a Ho: Nd-codoped fluoroindate fiber," *J. Light. Technol.*, vol. 41, no. 2, pp. 702–708, Jan. 2023, doi: 10.1109/JLT.2022.3218190.

[13] M. Kochanowicz et al., "Fluoroindate glass co-doped with Yb^{3+}/Ho^{3+} as a 2.85 μm luminescent source for Mid-IR sensing," *Sensors*, vol. 21, no. 6, Mar. 2021, Art. no. 2155, doi: 10.3390/s21062155.

[14] J. Swiderski and P. Grzes, "High-power mid-IR supercontinuum generation in fluoroindate and arsenic sulfide fibers pumped by a broadband 1.9-2.7 μm all-fiber laser source," *Opt. Laser Technol.*, vol. 141, Apr. 2021, Art. no. 107178, doi: 10.1016/j.optlastec.2021.107178.

[15] Z. Zhang et al., "Enhanced 3.9 μm emission from diode pumped Ho^{3+}/Eu^{3+} codoped fluoroindate glasses," *Opt. Lett.*, vol. 46, no. 9, pp. 2031–2034, May 2021, doi: 10.1364/OL.423399.

[16] P. Wang et al., "3.5 μm emission in Er^{3+} doped fluoroindate glasses under 635 nm laser excitation," *J. Lumin.*, vol. 237, May 2021, Art. no. 118200, doi: 10.1016/j.jlumin.2021.118200.

[17] H. He, Z. Jia, Y. Ohishi, W. Qin, and G. Qin, "Efficient ∼4 µm emission from Pr^{3+}/Yb^{3+} co-doped fluoroindate glass," *Opt. Lett.*, vol. 46, no. 22, pp. 5607–5610, Nov. 2021, doi: 10.1364/OL.440635.

[18] Z. Liu, J. She, and B. Peng, "Spectroscopic properties of Er^{3+}-doped fluoroindate glasses," *J. Rare Earths*, vol. 40, no. 7, pp. 1037–1042, Jul. 2022, doi: 10.1016/j.jre.2021.05.011.

[19] J. Cao et al., "Modeling and optimization of cascaded lasing in a holmium doped fluoride fiber laser with efficient output at 3.92 µm," *Opt. Exp.*, vol. 30, no. 18, pp. 31623–31633, Aug. 2022, doi: 10.1364/OE.468463.

[20] A. Annunziato, F. Anelli, P. L. P. Du Teilleul, S. Cozic, S. Poulain, and F. Prudenzano, "Fused optical fiber combiner based on indium fluoride glass: perspectives for mid-IR applications," *Opt. Exp.*, vol. 30, no. 24, pp. 44160–44174, Nov. 2022, doi: 10.1364/OE.471090.

[21] V. Portosi, D. Laneve, M. C. Falconi, and F. Prudenzano, "Advances on photonic crystal fiber sensors and applications," *Sensors*, vol. 19, no. 8, Apr. 2019, Art. no. 1892, doi: 10.3390/s19081892.

[22] M. R. Majewski, G. Bharathan, A. Fuerbach, and S. D. Jackson, "Long wavelength operation of a dysprosium fiber laser for polymer processing," *Opt. Lett.*, vol. 46, no. 3, pp. 600–603, Feb. 2021, doi: 10.1364/OL.417208.

[23] M. C. Falconi, D. Laneve, and F. Prudenzano, "Advances in mid-IR fiber lasers: tellurite, fluoride and chalcogenide," *Fibers*, vol. 5, no. 2, Jun. 2017, Art. no. 23, doi: 10.3390/fib5020023.

[24] A. Florez, Y. Messaddeq, O. L. Malta, and M. A. Aegerter, "Optical transition probabilities and compositional dependence of Judd-Ofelt parameters of Er^{3+} ions in fluoroindate glass," *J. Alloys Compounds*, vol. 227, no. 2, pp. 135–140, Sep. 1995, doi: 10.1016/0925-8388(95)01613-9.

[25] S. Sujecki et al., "Comparative modeling of infrared fiber lasers," *Photonics*, vol. 5, no. 4, Nov. 2018, Art. no. 48, doi: 10.3390/photonics5040048.

[26] M. C. Falconi, D. Laneve, V. Portosi, S. Taccheo, and F. Prudenzano, "Design of a multi-wavelength fiber laser based on Tm:Er:Yb:Ho codoped germanate glass," *J. Light. Technol.*, vol. 38, no. 8, pp. 2406–2413, Apr. 2020, doi: 10.1109/JLT.2020.2966999.

[27] A. D'Orazio et al., "Design of Er^{3+} doped SiO_2-TiO_2 planar waveguide amplifier," *J. Non Crystalline Solids*, vol. 322, no. 1, pp. 278–283, Jul. 2003, doi: 10.1016/S0022-3093(03)00215-1.

[28] Y. Wang et al., "Ultrafast Dy^{3+}: fluoride fiber laser beyond 3 μm," *Opt. Lett.*, vol. 44, no. 2, pp. 395–398, Jan. 2019, doi: 10.1364/OL.44.000395.

[29] L. Sojka et al., "High peak power Q-switched Er: ZBLAN fiber laser," *J. Light. Technol.*, vol. 39, no. 20, pp. 6572–6578, Oct. 2021, doi: 10.1109/JLT.2021.3099498.

[30] Y. Wang et al., "Mid-IR tunable CW and passively Q-switched laser operation of Dy-doped fluoride fiber," *Opt. Mater. Exp.*, vol. 12, no. 4, pp. 1502–1511, Apr. 2022, doi: 10.1364/OME.453046.

[31] R. I. Woodward, M. R. Majewski, and S. D. Jackson, "Mode-locked dysprosium fiber laser: Picosecond pulse generation from 2.97 to vol. 3.30 μm," *Appl. Phys. Lett. Photon.*, vol. 3, no. 11, Nov. 2018, Art. no. 116106, doi: 10.1063/1.5045799.

[32] G. Fornarelli, L. Mescia, F. Prudenzano, M. De Sario, and F. Vacca, "A neural network model of erbium-doped photonic crystal fibre amplifiers," *Opt. Laser Technol.*, vol. 41, no. 5, pp. 580–585, Jul. 2009, doi: 10.1016/j.optlastec.2008.10.010.

[33] T. Catunda, L. A. O. Nunes, A. Florez, Y. Messaddeq, and M. A. Aegerter, "Spectroscopic properties and upconversion mechanisms in Er^{3+}-doped fluoroindate glasses," *Phys. Rev. B*, vol. 53, no. 10, pp. 6065–6070, Mar. 1996, doi: 10.1103/PhysRevB.53.6065.

[34] I. Chiamenti et al., "First-order fiber Bragg grating inscription in indium fluoride fiber using a UV/Vis femtosecond laser and two-beam interferometry," *Opt. Lett.*, vol. 46, no. 8, pp. 1816–1819, Apr. 2021, doi: 10.1364/OL.420264.

[35] Z. Qin, Y. Zhou, G. Xie, P. Yuan, J. Ma, and L. Qian, "Red-diode-clad-pumped CW and mode-locked Er: ZBLAN fiber laser at 3.5 µm," *Opt. Exp.*, vol. 30, no. 7, pp. 11174–11180, Mar. 2022, doi: 10.1364/OE.454521.

Mario Christian Falconi received the M.Sc. degree in electronic engineering (*cum laude*) and the Ph.D. degree in electrical and information engineering from the Politecnico di Bari, Bari, Italy, in 2015 and 2019, respectively. In 2019, he was a Research Fellow and is currently a Research Assistant of electromagnetic fields with the Department of Electrical and Information Engineering, Politecnico di Bari. His research interests include fiber lasers and amplifiers, photonic crystal fibers, and nonlinear effects in optical fibers.

Antonella Maria Loconsole received the M.Sc. degree in telecommunications engineering (*cum laude*) in 2019 from the Politecnico di Bari, Bari, Italy, where she is currently working toward the Ph.D. degree in electrical and information engineering. Her research interests include SIW antennas, microwave applicators for medical applications, and optical fiber lasers and amplifiers.

Andrea Annunziato received the M.Sc. degree in electronic engineering (*cum laude*) in 2020 from the Politecnico di Bari, Bari, Italy, where he is currently working toward the Ph.D. degree in aerospace sciences and engineering. His research interests include optical fiber sensors, lasers, and amplifiers.

Solenn Cozic received the Ph.D. degree in material science from Rennes 1 University, Rennes, France, in 2016. She is currently a Research and Development Engineer with Le Verre Fluoré. Her research interests include development of novel fluoride glasses, optical fibers and fluoride glass fiber components for mid infrared, and visible fiber lasers applications.

Samuel Poulain received the Engineering master's degree from ENSTA ParisTech, Palaiseau, France, in 1997. After 15 years with Automotive Industry as an Engineer, he became the General Manager of Le Verre Fluoré in 2015. He is involved in various scientific developments, in particular in mid-IR supercontinuum generation and mid-IR fiber lasers.

Francesco Prudenzano (Member, IEEE) received the Ph.D. degree in electronic engineering from the Politecnico di Bari, Bari, Italy, in November 1996. Since 2018, he has been a Full Professor of electromagnetic fields with the Department of Electrical and Information Engineering, Politecnico di Bari. His research interests include the design and characterization of microwave devices, integrated optics, and optical fiber-based devices. He is the Head of the Microwave and Optical Engineering Group, Department of Electrical and Information Engineering, Politecnico di Bari. From 2017 to 2018, he was the Chair of SIOF, Italian Society of Optics and Photonics (Italian branch of EOS - European Optical Society). He has coauthored more than 400 publications, 295 of which got published in journals and international conferences, lectures, and invited papers. He is involved in several national and international research projects and cooperations.

Open Access funding provided by 'Politecnico di Bari' within the CRUI CARE Agreement